
Article:
Huang, L., Zhu, Z.Q. orcid.org/0000-0001-7175-3307, Feng, J. et al. (2 more authors) (2019) Comparative Analysis of Variable Flux Reluctance Machines With Double- and Single-Layer Concentrated Armature Windings. IEEE Transactions on Industry Applications, 55 (2). pp. 1505-1515. ISSN 0093-9994

https://doi.org/10.1109/TIA.2018.2884608

Comparative Analysis of Variable Flux Reluctance Machines with Double- and Single-layer Concentrated Armature Windings

L.R. Huang, Z.Q. Zhu, *Fellow, IEEE*
Department of Electronic and Electrical Engineering
The University of Sheffield, Sheffield S1 3JD, UK
lhuang18@sheffield.ac.uk, z.q.zhu@sheffield. ac.uk

J.H. Feng, S.Y. Guo, J.X. Shi
CRRC Zhuzhou Institute Co. Ltd
Shidai Road, Shifeng District, Zhuzhou, Hunan, China
fengjh@csrzic.com, guosy@csrzic.com, shijx2@csrzic.com

***Abstract*—In this paper, the variable flux reluctance machines (VFRMs) with double- and single-layer concentrated armature windings are comparatively analyzed. Firstly, the single-layer winding is found to have identical winding factor as double-layer winding, but significantly larger peak value of magneto-motive force, which will result in severe local saturation in cores of VFRMs with single-layer winding. Then, based on the magnetic gearing effect and finite element analysis, the electromagnetic performances of VFRMs with both winding types are compared. The VFRMs with single-layer winding are proved to be always lower in average torque, higher in torque ripple, larger in iron loss, and lower in efficiency than those with double-layer winding. Nevertheless, better fault tolerance capability is achieved for single-layer winding due to its physical separation between phases and larger phase self-inductance. Overall, the double-layer armature winding is the preferable choice for the VFRMs. Finally, a 6-stator-slot/4-rotor-pole VFRM with both double- and single-layer windings is prototyped for verification.**

Keywords*— *Double-layer concentrated winding, single-layer concentrated winding, reluctance machine.

I. INTRODUCTION

Variable flux reluctance machines (VFRMs) are one kind of magnetless machines [1]. Fig. 1(a) presents the configurations of a typical 6-stator-slot/4-rotor-pole (6s/4r) VFRM. They have robust structure, i.e., compact concentrated winding and simple rotor, which are similar to those of the switched reluctance machines (SRMs). Two sets of windings, i.e., AC-excited armature winding and DC-excited field winding, are both located at the stator, which avoids the requirement of slip-ring/brush [2].

In [3]-[12], the electromagnetic performance of VFRMs with double-layer concentrated (DLC) armature winding has been comprehensively investigated in terms of torque production mechanism [3][4], stator/rotor pole combination [5], vibration and acoustic noise [6], design and optimization method [7][8], power factor [9], efficiency envelope [10], torque ripple reduction methods [11], control scheme [12] and multi-phase feasibility [13]. The VFRMs are proved to be a good candidate for low cost and high fault tolerance applications.

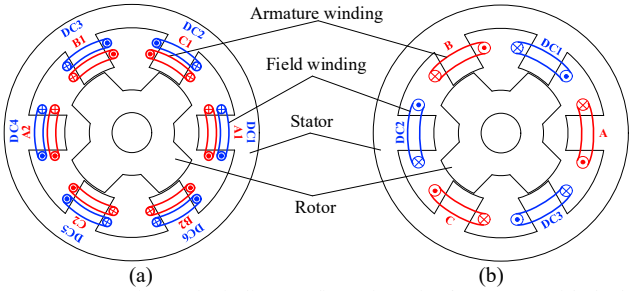

Fig. 1. Cross section and winding configuration of 6s/4r VFRM with double- and single-layer concentrated winding. (a) Double-layer winding. (b) Single-layer winding.

According to [4], it is proved that the torque production mechanism of VFRMs is based on the airgap flux modulation effect and can be greatly influenced by the harmonic content of magneto-motive-force (MMF), which is determined by the winding configurations. In this paper, the influence of winding configurations on the performance of VFRMs is further investigated. Since the concentrated winding type is essential for VFRMs to ensure their robustness and simplicity, this feature is kept during the investigation. In this case, apart from the DLC winding, the single-layer concentrated (SLC) winding is another potential candidate for armature winding.

In fact, the application of SLC winding in electrical machines is not a new concept. In [14]-[16], the SLC winding is applied to permanent magnet (PM) machines. Compared with DLC winding, the SLC winding is found to contain more subharmonics, which will eventually influence the back-EMF and inductance of PM machines. In [17] and [18], the SLC winding is also applied to the SRMs excited by unipolar rectangular and sinusoidal excitations. The machines with SLC winding are found to have higher torque density than those with DLC winding at low current density condition and are able to boost fault tolerance. In [19], the performance of VFRMs with SLC winding is analyzed by finite element analysis (FEA). It is found that the 6s/7r is the best stator/rotor pole combination for VFRMs with SLC winding.

Up to now, the performances of VFRMs with DLC and SLC armature windings are investigated separately and have not been compared. Hence, to find out the preferable winding

type for VFRMs, [20] comprehensively explain the performance discrepancy between these two winding types based on the magnetic gearing effect and FEA. The 6s- and 12s- VFRMs are selected as examples during the investigation. The revealed conclusions are general and applicable to VFRMs with other stator/rotor pole combinations. In this paper, the investigation is further extended by comparing efficiency and fault tolerance of VFRMs with two winding types. Moreover, more experimental results are added.

The paper is organized as follows: In section II, the winding factor, MMF and feasible stator/rotor pole combination of DLC and SLC windings are compared. In Section III, the average torque and torque ripple performance of VFRMs with both winding types are investigated using magnetic gearing effect. In Section IV, the efficiency and fault tolerance are extensively compared. In Section V, a 6s/4r VFRM prototype with DLC and SLC windings are tested.

II. Winding Factor, MMF and Feasible Stator/Rotor Pole Combination Comparison

A. Armature winding

As presented in Fig. 2, the DLC armature winding can be configured into 6-stator-slots/2-poles (6s/2p) and 6s/4p types, whereas the SLC winding only has one configuration. The normalized MMF distributions of both DLC and SLC windings are shown in Fig. 3. It can be found that:

(a) The peak value of MMF of SLC winding is twice of that of DLC winding.

(b) The 6s/2p and 6s/4p DLC windings contain $|6n\pm1|$-th and $|6n\pm2|$-th harmonics, respectively, whereas the SLC winding contains all the harmonics except those with $3n$-th order. In addition, due to the identical winding factor (see Table I), the magnitudes of the MMF harmonics of DLC winding are equal to their counterparts of SLC winding which have the same harmonic order.

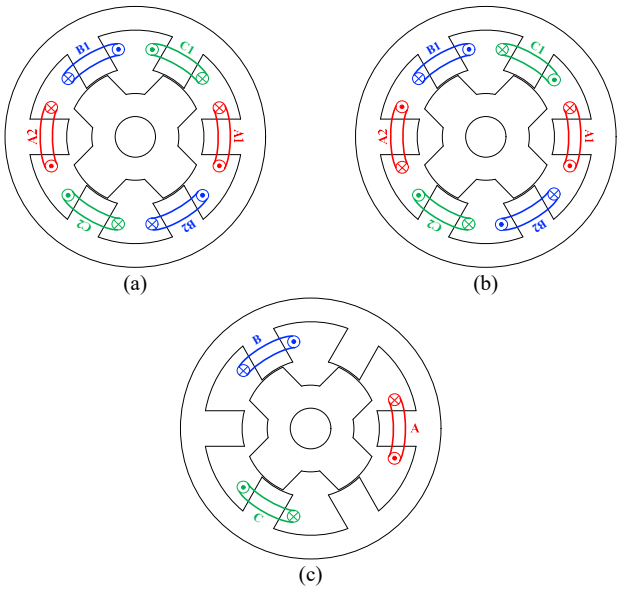

Fig. 2. Configurations of double- and single-layer armature winding. (a) DLC winding 6s/2p. (b) DLC winding 6s/4p. (c) SLC winding.

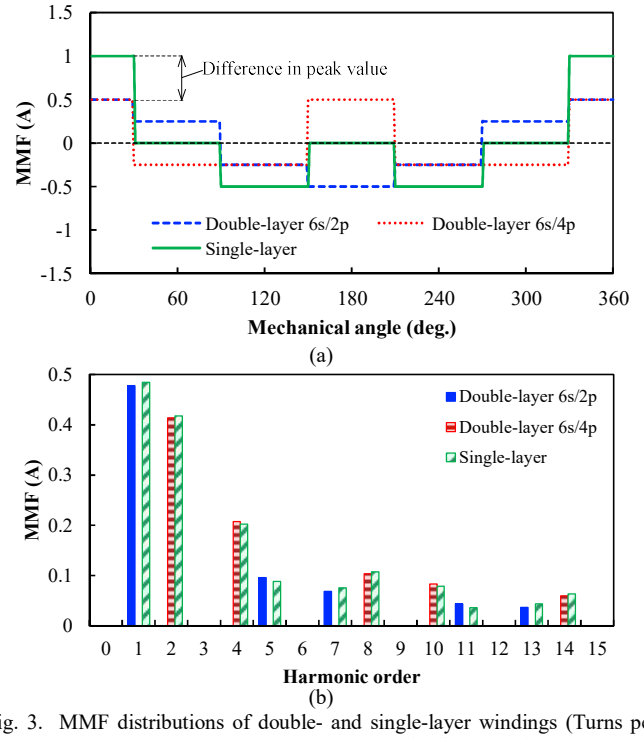

Fig. 3. MMF distributions of double- and single-layer windings (Turns per slot is 72, (I_A, I_B, I_C) is (2A,-1A,-1A)). (a) MMF distributions. (b) Spectra.

TABLE I
Winding Factors of Double- and Single-Layer Armature Windings

Winding factor		DLC		SLC
		6s/2p	6s/4p	
Pitch factor	K_{pn}	sin($n\pi$/6)		
Distribution factor	K_{dn}	1		
Winding factor	K_{dpn}	sin($n\pi$/6)		
Harmonic order		**DLC**		**SLC**
		6s/2p	**6s/4p**	
1st		0.5	-	0.5
2nd		-	0.866	0.866
3rd		-	-	-
4th		-	0.866	0.866
5th		0.5	-	0.5
6th		-	-	-
7th		0.5	-	0.5
8th		-	0.866	0.866
9th		-	-	-
10th		-	0.866	0.866

B. Field winding

For field winding, there are two configurations, as shown in Fig. 4. These two configurations are identical from the electromagnetic point of view since the current polarity distributions in slots are the same. However, their physical connections are different. The all-tooth-wound field winding is more suitable for double-layer armature winding VFRM since all the teeth have even windings wound. For the same reason, the alternative-tooth-wound field winding is more suitable for single-layer armature winding.

The MMF distributions of these two configurations are the same and presented in Fig. 5. It can be seen that the MMF of field winding contains $|6m+3|$-th harmonics.

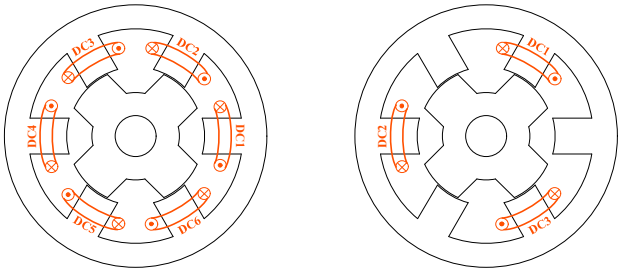

(a) (b)

Fig. 4. Configurations of field winding. (a) All-tooth-wound winding. (b) Alternative-tooth-wound winding.

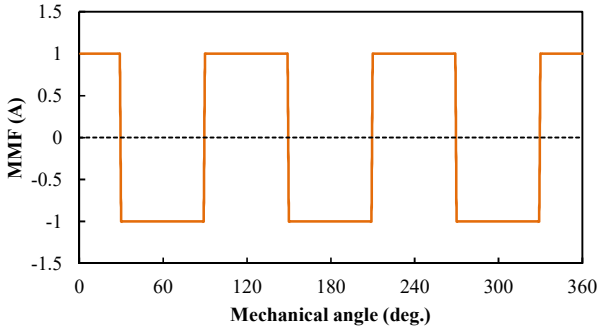

(a)

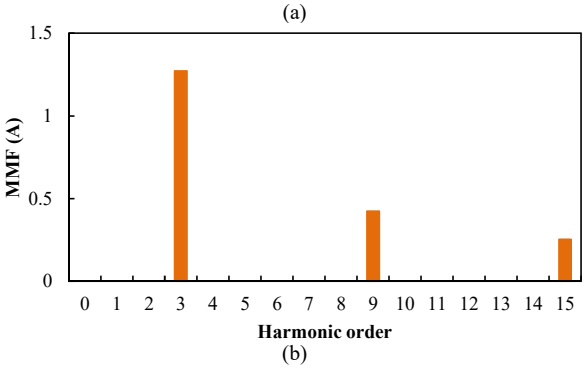

(b)

Fig. 5. MMF distributions of field windings (Turns per slot is 72, I_{dc} is 2A). (a) MMF distributions. (b) Spectra.

TABLE II
ORDERS AND ROTATING SPEEDS OF THE MMF HARMONICS FOR ARMATURE AND FIELD WINDINGS

Winding types			Harmonic order	Rotating speed
Armature winding	DLC	6s/2p	$\|6n+1\|$	$^{*}N_r\Omega_r$
			$\|6n-1\|$	$-N_r\Omega_r$
		6s/4p	$\|6n+2\|$	$N_r\Omega_r$
			$\|6n-2\|$	$-N_r\Omega_r$
	SLC	6s/4p	$\|6n+1\|$ & $\|6n-2\|$	$N_r\Omega_r$
			$\|6n-1\|$ & $\|6n+2\|$	$-N_r\Omega_r$
Field winding	-		$\|6m+3\|$	0

* N_r-Rotor pole number, Ω_r-Rotor rotating speed

TABLE III
FEASIBLE ROTOR POLE NUMBER FOR VFRMS WITH DOUBLE- AND SINGLE-LAYER WINDING

Armature winding		Feasible rotor pole number	Specific rotor pole number
DLC	6s/2p	$N_r=\|P_a\pm P_f\|=\|(6n\pm1)\pm(6m+3)\|=\|6k\pm2\|$	2, 4, 8,…
	6s/4p	$N_r=\|P_a\pm P_f\|=\|(6n\pm2)\pm(6m+3)\|=\|6k\pm1\|$	5, 7, 11,…
SLC		$N_r=\|P_a\pm P_f\|=\|(6n\pm1)\pm(6m+3)\|=\|6k\pm2\|$ & $N_r=\|P_a\pm P_f\|=\|(6n\pm2)\pm(6m+3)\|=\|6k\pm1\|$	2, 4, 5, 7, 8,…

C. *Feasible rotor pole number*

According to [4], the principle of feasible rotor pole number selection is given by (1).

$$N_r = \left|P_a \pm P_f\right| \tag{1}$$

where N_r the rotor pole number; P_a and P_f are the harmonic orders of armature and field winding MMFs, respectively.

From the foregoing investigation, the orders and corresponding rotating speeds of armature and field winding MMF components are identified in Table II. Consequently, the feasible rotor pole number for VFRMs with both double- and single-layer armature windings is deduced in Table III. All the integers except the multiples of 3 can be chosen as the rotor pole numbers for VFRMs with DLC and SLC windings, which is also confirmed by FEA in [5] and [19].

III. TORQUE PERFORMANCE COMPARISON

A. *Torque performance estimation method*

According to [4], the torque productions of VFRMs are originated from the interactions between AC and AC currents, DC and DC currents, and AC and DC currents, as shown in the torque expression (2). They are normally nominated as reluctance torque T_r, cogging torque T_c, and synchronous torque T_s in regular electric machines.

$$\begin{aligned} T_e(t) = &-R_{si}L_{stk}\int_0^{2\pi}\frac{\Lambda_r(\theta,t)}{2}\frac{dF_{sa}^2(\theta,t)}{d\theta} - && ①\ T_r \\ &R_{si}L_{stk}\int_0^{2\pi}\frac{\Lambda_r(\theta,t)}{2}\frac{dF_{sf}^2(\theta,t)}{d\theta} - && ②\ T_c \\ &R_{si}L_{stk}\int_0^{2\pi}\Lambda_r(\theta,t)\frac{d\left[F_{sa}(\theta,t)F_{sf}(\theta,t)\right]}{d\theta} && ③\ T_s \end{aligned} \tag{2}$$

where R_{si} is the radius of stator inner surface; L_{stk} is the stack length of the machine; θ is the mechanical angle in the stator reference frame; Λ_r is the rotor permeance, which is the radial airgap permeance of slotted rotor and slotless stator model; F_{sa} and F_{sf} are the "modulated MMFs" of armature and field currents, respectively. They are defined by (3).

$$\begin{cases} F_{sa}(\theta,t) = F_a(\theta,t)g_0\Lambda_s(\theta)/\mu_0 \\ F_{sf}(\theta,t) = F_f(\theta,t)g_0\Lambda_s(\theta)/\mu_0 \end{cases} \tag{3}$$

where F_a and F_f are the original MMFs of armature and field currents, respectively; g_0 is the airgap length; μ_0 is the permeability of vacuum; and $\Lambda_s(\theta)$ is the stator permeance, which is the radial airgap permeance of slotted stator and slotless rotor model, i.e.,

$$\Lambda_s(\theta) = \Lambda_{s0} + \sum_{k=1}^{\infty}\Lambda_{sk}\cos(kN_s\theta) \tag{4}$$

where Λ_{s0} and Λ_{sk} are the magnitudes of the dc and the k-th harmonic of stator permeance; N_s is the stator slot number. The coefficient calculation of stator permeance can be found in [4].

As proved in [4], the torque performance of VFRMs can be estimated by using magnetic gearing effect. The armature and field modulated MMFs act as the outer and inner magnets of a magnetic gear, whereas the rotor permeance components are equivalent to the iron modulators of a magnetic gear.

Considering the fact that the modulated MMFs and rotor permeance contains loads of harmonics, the torque production of VFRMs is actually a combination of various "magnetic gear pairs". The orders of rotor permeance P_r and modulated MMFs harmonics (P_m, P_n) should satisfy condition (5) to constitute a specific "magnetic gear pair".

$$P_r = |P_m \pm P_n| \tag{5}$$

where P_r is the harmonic orders of rotor permeance; P_m and P_n are the harmonic orders of modulated MMFs and could be either from armature or field modulated MMF. The sources of P_m and P_n determine which torque component the magnetic gear pair contributes to. For instance, when P_m and P_n both stand for the harmonic orders of armature modulated MMF, this magnetic gear pair belongs to the reluctance torque.

Moreover, the magnetic gear pairs will contribute to either average torque or torque ripple production depending on whether it satisfies the rotating speed condition (6).

$$P_r\Omega_r = \mathrm{sgn}(P_m \pm P_n)(\Omega_m \pm \Omega_n) \tag{6}$$

where sgn is sign function; the (Ω_m, Ω_n) are the rotating speeds of (P_m, P_n)-th modulated MMFs. If one magnetic gear pair satisfies condition (6), it will contribute to the average torque of its corresponding torque component. Otherwise, it will only lead to torque ripple in its corresponding torque component. The frequency of the ripple for a specific magnetic gear pair is:

$$f_{ripple} = \left[\frac{P_r}{N_r} - \frac{\mathrm{sgn}(P_m \pm P_n)(\Omega_m \pm \Omega_n)}{N_r\Omega_r}\right] f_0 \tag{7}$$

where f_0 is the frequency of AC current.

By using the method mentioned above, it is possible to estimate the average torque and torque ripple performances of each torque component for VFRMs once the harmonic contents of rotor permeance and modulated MMFs are obtained.

For the rotor permeance, it can be expressed as

$$\Lambda_r(\theta,t) = \Lambda_{r0} + \sum_{k=1}^{\infty} \Lambda_{rk} \cos\left[kN_r(\theta - \Omega_r t - \theta_{r0})\right] \tag{8}$$

where Λ_{r0} and Λ_{rk} are the magnitudes of the dc and k-th harmonics of the rotor permeance, respectively; θ_{ro} is the initial position of the rotor. The coefficient calculation of rotor permeance can be found in [4]. Thus, the harmonic content of rotor permeance can be concluded in Table IV.

TABLE IV
ORDERS AND ROTATING SPEEDS OF ROTOR PERMEANCE HARMONICS

Rotor permeance harmonics	Harmonic order	Rotating speed
	P_r	Ω
Λ_{r0}	0	0
Λ_{rk}	kN_r	$kN_r\Omega_r$

Regarding the modulated MMF, its relationship with the original MMF is illustrated in [4]. It is proved that these two types of MMFs are identical in terms of harmonic orders and corresponding rotating speeds, albeit with modified harmonic magnitudes due to the modulation effect of stator permeance. In this case, the harmonic contents of modulated MMFs can be directly derived from the original MMFs, which are already presented in Table II.

By synthesizing Tables II and IV, and conditions (5)-(8), the magnetic gear pairs of the torque components for all the VFRMs with DLC and SLC windings can be identified. For clarity, the 6s/4r and 6s/5r VFRMs with DLC and SLC windings are selected as examples in the following investigations. The revealed conclusions will be extended to all the VFRMs afterward.

B. Average torque performance

By only considering the dominant components of modulated MMFs (harmonics with orders lower than 10), the magnetic gear pairs which contribute to the average torque for 6s/4r and 6s/5r VFRMs are listed in Table V.

TABLE V
MAGNETIC GEAR PAIRS OF AVERAGE TORQUE PRODUCTION FOR 6S/4R AND 6S/5R VFRMS WITH DOUBLE- AND SINGLE-LAYER ARMATURE WINDINGS

VFRM		Average torque	Λ_{rk}	P_r	Source-harmonic order	
					P_m	P_n
6s/4r	DLC	T_{s_avg}	Λ_{r1}	4	A-1	F-3
					A-7	F-3
		T_{r_avg}	Λ_{r2}	8	A-1	A-7
		T_{c_avg}	-	-	-	-
	SLC	T_{s_avg}	Λ_{r1}	4	A-1	F-3
					A-7	F-3
		T_{r_avg}	Λ_{r2}	8	A-1	A-7
					A-4	F-4
		T_{c_avg}	-	-	-	-
6s/5r	DLC	T_{s_avg}	Λ_{r1}	5	A-2	F-3
					A-8	F-3
		T_{r_avg}	Λ_{r2}	10	A-2	A-8
		T_{c_avg}	-	-	-	-
	SLC	T_{s_avg}	Λ_{r1}	5	A-2	F-3
					A-8	F-3
		T_{r_avg}	Λ_{r2}	10	A-2	A-8
					A-5	A-5
		T_{c_avg}	-	-	-	-

*A-Modulated MMF of armature current, F_{sa}
†F-Modulated MMF of field current, F_{sf}
-Additional magnetic gear pairs of VFRMs with single-layer winding

Some features can be revealed:

(a) The average torque of VFRMs with both winding types is generated by synchronous torque and reluctance torque components. Moreover, the synchronous torque and reluctance torque are proportional to the 1st and 2nd rotor permeance components, respectively. For a conventional salient pole rotor, the 1st component is much larger than the 2nd component [4]. Hence, the synchronous torque is the dominant one in average torque production, whereas the reluctance torque is negligible.

(b) The synchronous torque components of VFRMs with both winding types contain exactly the same magnetic gear pairs. Since the magnitudes of MMF harmonics are identical for double- and single-layer windings (see Section II), the synchronous torque productions of machines with both winding types are similar to each other. In contrast, the reluctance torque productions are different for machines with DLC and SLC windings. In comparison with the VFRMs with DLC winding, there are additional magnetic gear pairs in the reluctance torque components of the machines with SLC winding, as marked by grey color in Table V. This will lead to

larger reluctance torque for machines with SLC winding. However, as mentioned above, the reluctance torque is negligible in average torque production. Hence, this enhancement in reluctance torque is also minor. Consequently, the torque capabilities are similar for VFRMs with both winding types under magnetically unsaturated condition.

To verify this, the FEA results of four VFRMs (6s/4r-DLC, 6s/4r-SLC, 6s/5r-DLC, 6s/5r-SLC) are presented. The main dimensions of four machines are listed in Table VI. Fig. 6 shows the variations of average and reluctance torques with the advanced current angle under linear condition (magnetically unsaturated). It can be seen that the optimal advanced current angle of all four machines are close to 0 deg., which means the reluctance torques are relatively small for VFRMs. In addition, the peak average torque and reluctance torque of VFRMs with SLC winding is slightly larger than that of VFRMs with DLC winding. However, the difference between them is quite minor. This verifies the aforementioned conclusions.

TABLE VI
MAIN SPECIFICATIONS OF 6S/4R AND 6S/5R VFRMS

Parameters	Unit	VFRM			
		6s/4r		6s/5r	
		DLC	SLC	DLC	SLC
Stator outer diameter	mm	90			
Airgap length	mm	0.5			
Rated copper loss	W	30			
Rated current density	A/mm^2	6			
Rated power	W	70			
Rated speed	rpm	800			
Turns per slot (AC/DC)	-	183/183			
Split ratio	-	0.5		0.52	
Stator pole arc	deg.	27		24	
Rotor pole arc	deg.	34.6		26	

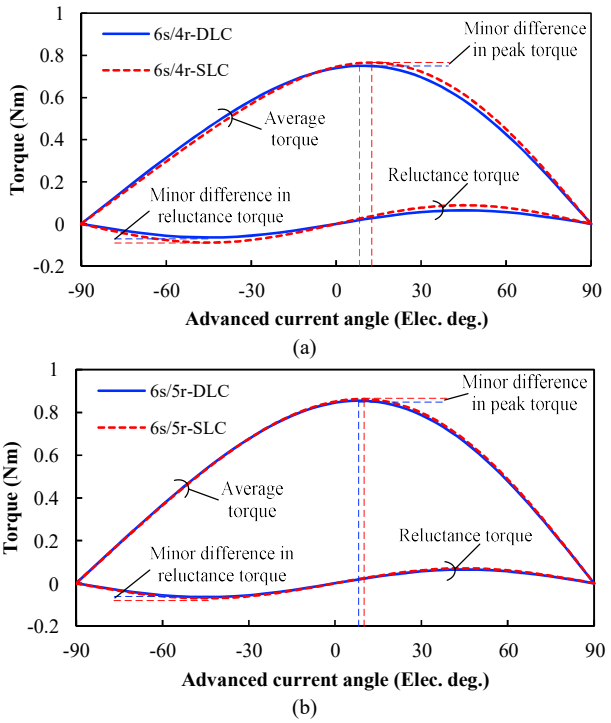

Fig. 6. Variations of average torque and reluctance torque of VFRMs with double- and single-layer armature windings under magnetically unsaturated condition (P_{cu}=30W). (a) 6s/4r VFRMs. (b) 6s/5r VFRMs.

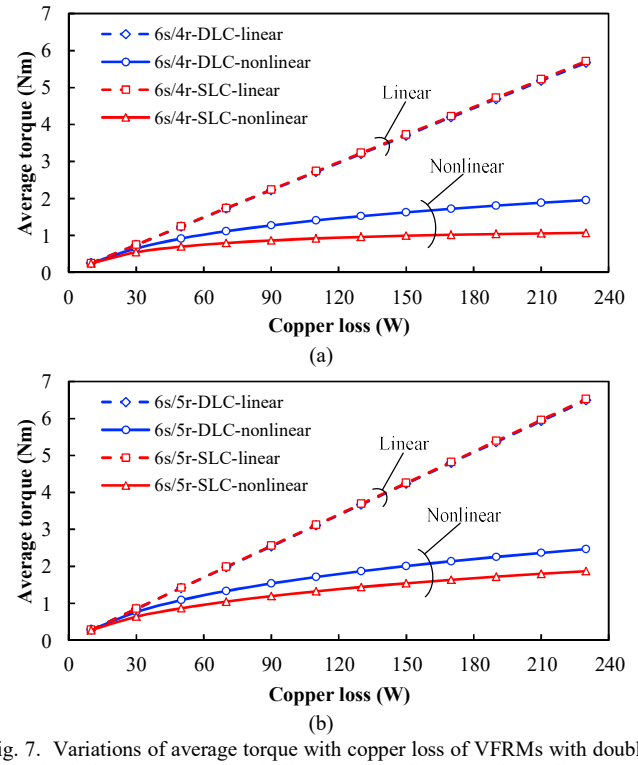

Fig. 7. Variations of average torque with copper loss of VFRMs with double- and single-layer armature windings under linear and nonlinear core conditions. (a) 6s/4r VFRMs. (b) 6s/5r VFRMs.

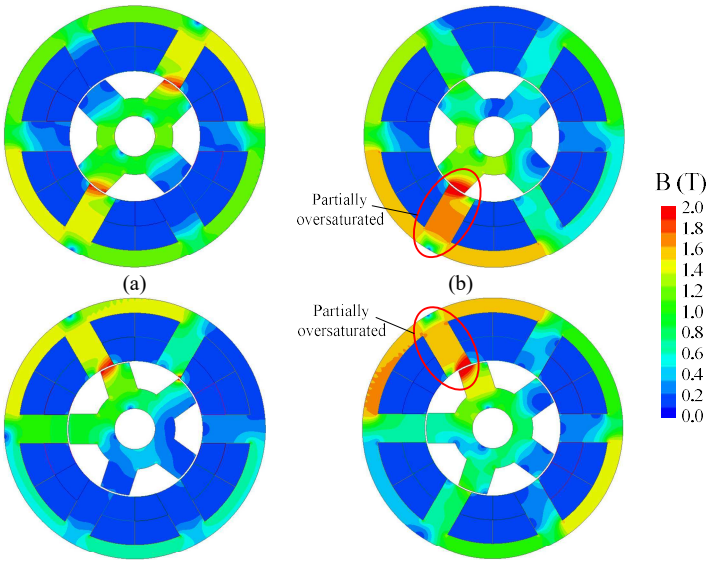

Fig. 8. Field distributions of VFRMs with double- and single-layer windings. (P_{cu}=30W) (a) 6s/4r-DLC VFRMs. (b) 6s/4r-SLC VFRMs. (c) 6s/5r-DLC VFRMs. (d) 6s/5r-SLC VFRMs.

Further, the influence of core saturation should be taken into account. The core material is set to nonlinear and the variations of average torques against copper loss are presented in Fig. 7. Compared with the linear case, a significant drop in average torque is observed when the core is saturated. Moreover, the average torque of VFRMs with SLC winding is always lower than that of the VFRMs with DLC winding under nonlinear condition. This is mainly due to the severer saturation status in cores of VFRMs with SLC winding. As

presented in Fig. 3, the peak value of MMF of SLC winding is twice of that of DLC winding under the same current setting, which will lead to local over-saturation in cores, as confirmed by the field distributions of 6s/4r and 6s/5r VFRMs in Fig. 8.

Overall, the average torque of VFRMs with SLC winding is always lower than those with DLC winding.

C. Torque ripple performance

Similarly, Table VII shows the magnetic gear pairs of torque ripple in VFRMs. Some features can be found:

(a) The reluctance torque is the main source of torque ripple.

(b) Compared with VFRMs with DLC winding, there are additional magnetic gear pairs in the synchronous and reluctance torque components of VFRMs with SLC windings, which will lead to additional torque ripple in these two torque components. Moreover, this additional ripple of reluctance torque is proportional to the 1st rotor permeance. Hence, the reluctance torque ripple of VFRMs with SLC winding is significantly larger than that of VFRMs with DLC winding.

(c) The torque ripple frequencies of 6s/4r-DLC and 6s/5r-DLC VFRMs are $3f_0$ and $6f_0$, respectively. In contrast, due to the additional magnetic gear pairs in synchronous and reluctance torque, the torque ripple frequencies of the VFRMs with SLC windings are always $3f_0$.

To verify these features, the total and reluctance torque waveforms of 6s/4r and 6s/5r VFRMs are calculated by FEA, as presented in Figs. 9 and 10. It can be seen that the ripples of total and reluctance torques of VFRMs with SLC windings are significantly larger than those of VFRMs with DLC windings. In addition, the frequencies of torque ripples of VFRMs with both winding types match the predictions.

D. Influence of stator/rotor pole combination

In the foregoing investigation, the 6s/4r and 6s/5r VFRMs with DLC and SLC windings are analyzed. For VFRMs with other stator/rotor pole combinations, the same method can also be applied. The torque features are concluded as:

(a) The average torque of VFRMs with SLC winding is always smaller than VFRMs with DLC winding.

(b) The torque ripple of VFRMs with SLC winding is always larger than VFRMs with DLC winding.

(c) The torque ripple frequencies of VFRMs with DLC winding are $6f_0$, except those with $(6j)$s/$[(6i\pm2)j]$r (i, j=0, 1, 2…) stator/rotor pole combinations (the torque ripple frequencies of these VFRMs are $3f_0$). In contrast, the torque ripple frequencies of VFRMs with SLC winding are always $3f_0$.

To verify this, the 6s/(2~14)r VFRMs with DLC and SLC armature windings are globally optimized under the same constraint listed in Table VIII to achieve the maximal average torque. Their average torque and torque ripple are compared in Fig. 11. The results agree the prediction of investigation well. Moreover, the 6s/7r stator/rotor pole combination is found to be the best for VFRMs with both DLC and SLC armature windings, as also confirmed in [7] and [19].

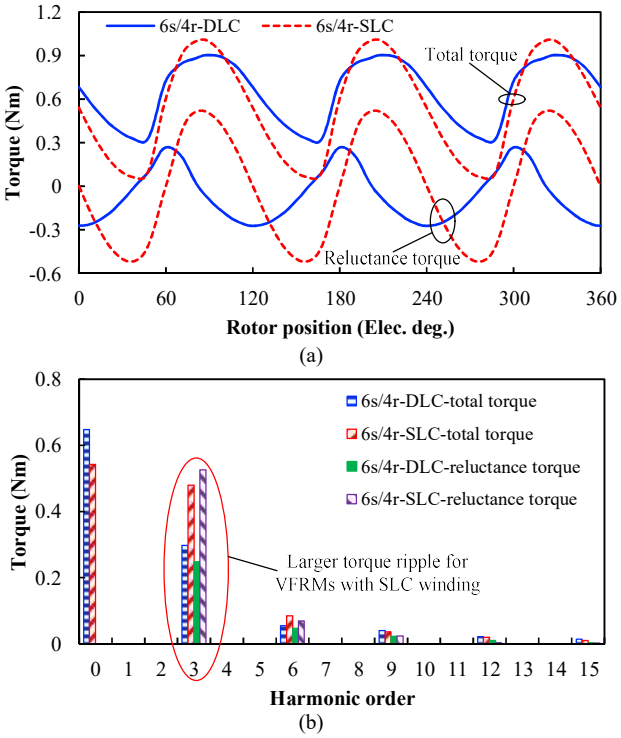

Fig. 9. Total and reluctance torque waveforms of 6s/4r VFRM with double- and single-layer windings (P_{cu}=30W). (a) Torque waveforms. (b) Spectra.

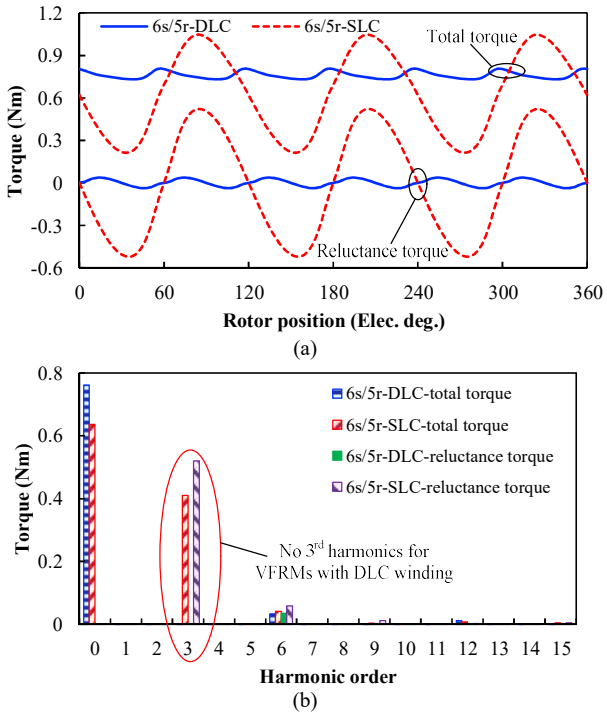

Fig. 10. Total and reluctance torque waveforms of 6s/5r VFRM with double- and single-layer windings (P_{cu}=30W). (a) Torque waveforms. (b) Spectra.

TABLE VII
MAGNETIC GEAR PAIRS OF TORQUE RIPPLE PRODUCTION FOR 6S/4R AND 6S/5R VFRMS WITH DOUBLE- AND SINGLE-LAYER ARMATURE WINDINGS

VFRM		Average torque	Λ_{rk}	P_r	Source-harmonic order		f_{ripple}
					P_m	P_n	
6s/4r	DLC	T_{s_ripple}	Λ_{r2}	8	A-5	F-3	$3f_0$
		T_{r_ripple}	Λ_{r1}	4	A-1	A-5	$3f_0$
		T_{c_ripple}	Λ_{r3}	12	F-3	F-9	$3f_0$
	SLC	T_{s_ripple}	Λ_{r2}	8	A-5	F-3	$3f_0$
		T_{r_ripple}	Λ_{r1}	4	A-1	A-5	$3f_0$
					A-2	A-2	$3f_0$
					A-4	A-8	
		T_{c_ripple}	Λ_{r3}	12	F-3	F-9	$3f_0$
6s/5r	DLC	T_{s_ripple}	Λ_{r5}	25	A-16	F-9	$6f_0$
		T_{r_ripple}	Λ_{r4}	20	A-10	A-10	$6f_0$
		T_{c_ripple}	Λ_{r6}	30	F-15	F-15	$6f_0$
	SLC	T_{s_ripple}	Λ_{r5}	25	A-16	F-9	$6f_0$
			Λ_{r2}	10	A-7	F-3	$3f_0$
		T_{r_ripple}	Λ_{r4}	20	A-10	A-10	$6f_0$
			Λ_{r1}	5	A-1	A-4	$3f_0$
					A-2	A-7	
		T_{c_ripple}	Λ_{r6}	30	F-15	F-15	$6f_0$

-Additional magnetic gear pairs of VFRMs with single-layer winding

TABLE VIII
CONSTRAINTS OF GLOBAL OPTIMIZATION

Parameters	Unit	Value
Stator outer diameter	mm	90
Airgap length	mm	0.5
Total copper loss	W	30
Turns per slot (AC/DC)	-	72/72

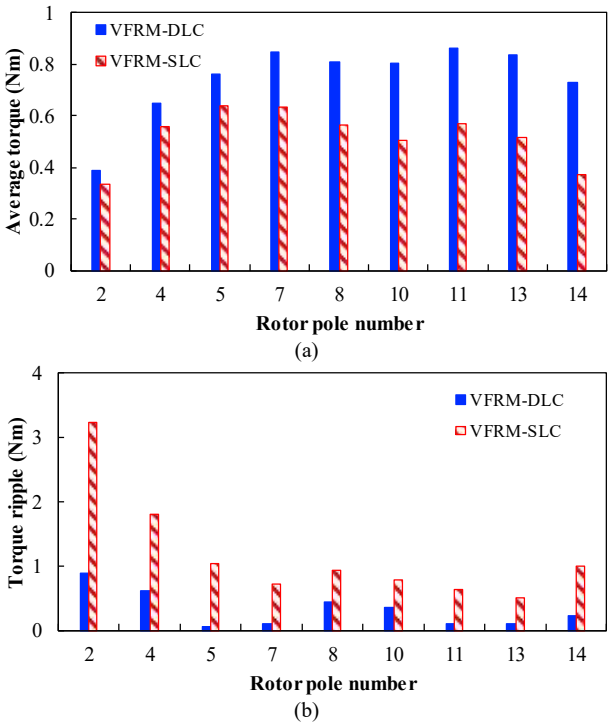

Fig. 11. Average torque and torque ripple of VFRMs with different rotor pole number (P_{cu}=30W). (a) Average torque. (b) Torque ripple.

IV. EFFICIENCY AND FAULT TOLERANCE COMPARISON

A. Efficiency

The efficiency of VFRMs is closely related to the iron loss and copper loss. Since both DLC and SLC armature windings are of concentrated winding type, the length of their end windings are similar to each other, which means the copper losses of these two winding types are also similar to each other under the same ampere turns of excitation. Therefore, the efficiencies of VFRMs with both winding types are mostly influenced by the iron loss.

According to Section II, it is proved that the MMF of single-layer winding contains more subharmonics than that of double-layer winding. This will lead to more harmonics in the airgap field and eventually larger iron loss in cores. By using the ANSYS Maxwell package, the iron losses and efficiencies of 6s/4r VFRMs can be calculated, as shown in Fig. 12. It can be found that the VFRM with DLC winding shows smaller iron loss and higher efficiency than that with SLC winding.

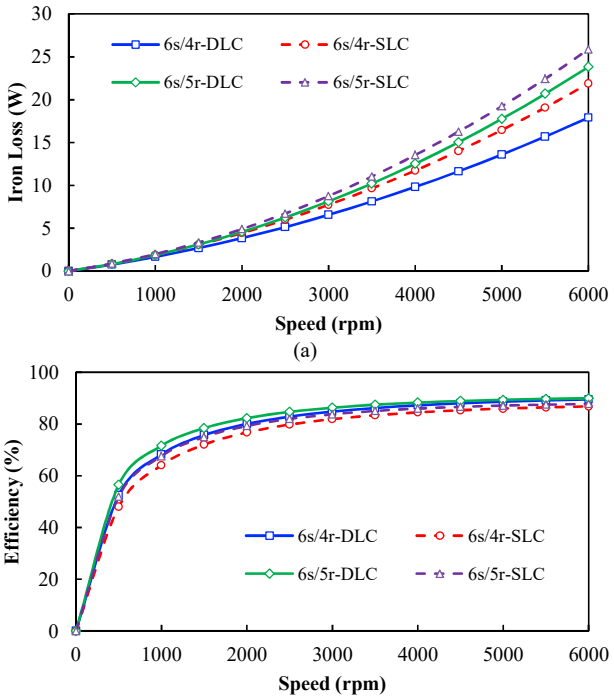

Fig. 12. Iron loss and efficiency of VFRMs with double- and single-layer armature windings (P_{cu}=30W). (a) Iron loss. (b) Efficiency.

B. Fault tolerance

VFRMs have high fault tolerance due to their simple structures. However, the phase short circuit and phase-to-phase faults are still risky. Regarding the phase short circuit, its main hazard comes from the large current under a fault condition. The amplitude of the current is influenced by the resistance and inductance of the armature winding. By using FEA and frozen permeability method [21], the self-inductance of phase A L_a and the mutual inductance between phase A and field winding M_{af} for 6s/4r VFRMs with both winding types are compared in Fig. 13. It can be seen that the mutual inductance of SLC winding is slightly smaller than that of DLC winding due to its severe local saturation. In contrast, the phase self-inductance of

SLC winding is significantly larger than that of DLC winding, which leads to smaller phase short-circuit current. Moreover, there is physical insulation between each phase for SLC winding, which will reduce the risk of phase-to-phase fault. Overall, the SLC winding has better fault tolerance capability than the DLC winding.

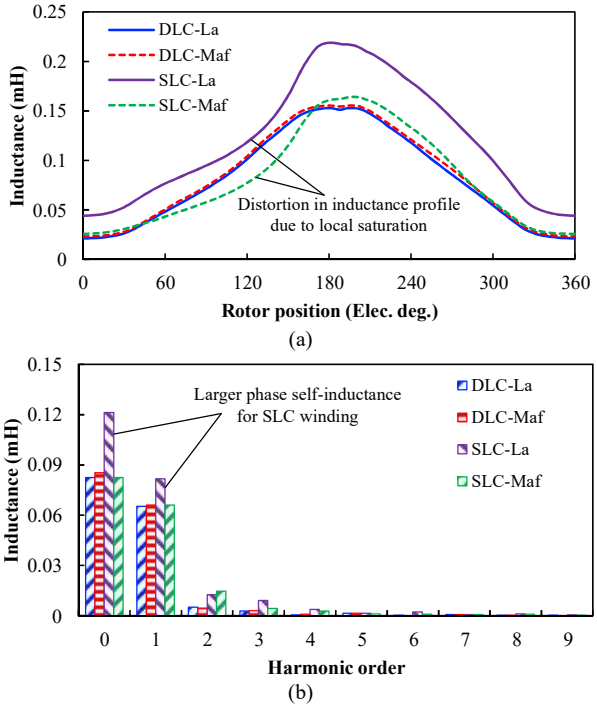

Fig. 13. Self-inductance of phase A and mutual inductance between armature and field winding for 6s/4r VFRMs with DLC and SLC windings (P_{cu}=30W). (a) Variations against rotor position. (b) Spectra.

V. Experimental Verification

In order to verify the analysis, a 6s/4r VFRM is prototyped, as shown in Fig. 14. The detailed dimension is shown in Table VI. The prototype machine has 2 coils wounded on each tooth with open terminals, which makes it flexible to change the winding connection from DLC to SLC winding, as shown in Fig. 15. The test rig is constructed by a DC machine, a torque transducer and the prototype. By using this rig, both open circuit and on load performance of the prototype is measured.

Firstly, the back-EMFs of VFRMs with DLC and SLC winding connections are measured when only DC current is injected at 400rpm, as shown in Fig. 16. The measured results match the FEA prediction well. Moreover, the back-EMFs of VFRM with DLC and SLC windings are almost identical to each other, as confirmed by their spectra. Hence, the torque capabilities of VFRMs with both winding configurations are also expected to be similar to each other without considering the influence of armature reaction and core saturation.

Then, by using the torque transducer, the transient torque waveforms are measured when DC current is 1.06A and AC current is 1.5A, as shown in Fig. 17. The torque measurement is conducted at a low speed (100rpm) to keep a stable current and avoid the influence of PWM as much as possible. The measured torque profiles have good agreement with the FEA predictions, albeit with some small fluctuations caused by the

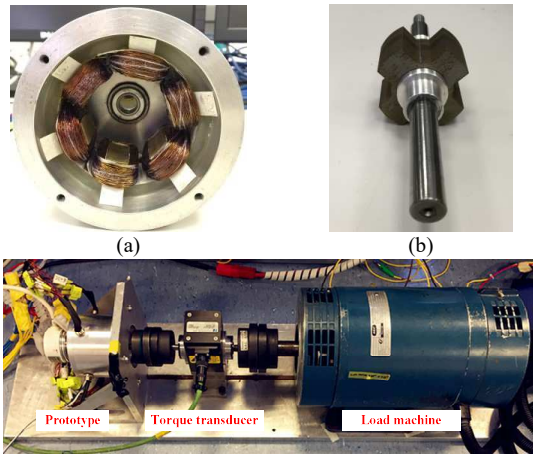

Fig. 14. Photos of 6s/4r VFRM prototype. (a) Stator. (b) Rotor. (c) Test rig.

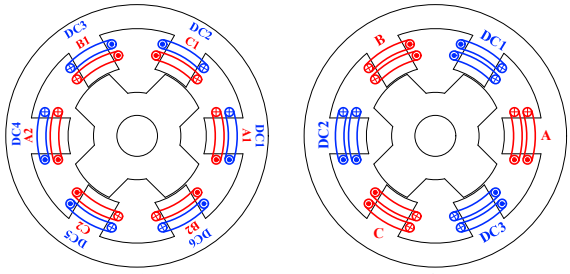

Fig. 15. Winding connections of 6s/4r VFRM prototypes with double- and single-layer armature windings. (a) DLC winding. (b) SLC winding.

minor spikes in current. In addition, as predicted, the torque ripple of VFRM with SLC winding is significantly larger than that of VFRM with DLC winding.

Fig. 18 further shows the variations of average torque with total RMS current for VFRM with both winding types. It is confirmed that DLC and SLC windings have similar average torque under light load condition. However, DLC winding has better overload capability than the SLC winding.

Finally, the efficiencies of VFRMs with DLC and SLC windings are measured. Firstly, the dynamic terminal voltage and current waveforms are measured by voltage and current clamps, as shown in Fig. 19. There are many spikes in both voltage and current signals. It is due to the PWM and measurement error of the voltage and current clamps. By taking the spectra of the phase voltage and current waveforms, the input power can be calculated by the fundamental voltage and current components. Then, the efficiency of VFRMs can be calculated by measuring the output torque simultaneously:

$$\eta = \frac{T\Omega_r}{3UI\cos(\Delta\varphi)} \tag{9}$$

where η is the efficiency; T is the output torque; U and I are the fundamental components of phase voltage and current; $\Delta\varphi$ is the phase shift between voltage and current.

The efficiencies at 400rpm and 800rpm are measured. There are big errors between FEA and measurement results, as shown in Table IX. This is mainly due to the measurement error since the prototype machines are very low in power and

the mechanical frictional loss is not considered in the prediction which can cause large errors. Nevertheless, the VFRM with DLC winding shows higher efficiency than that with SLC winding, confirming the analysis.

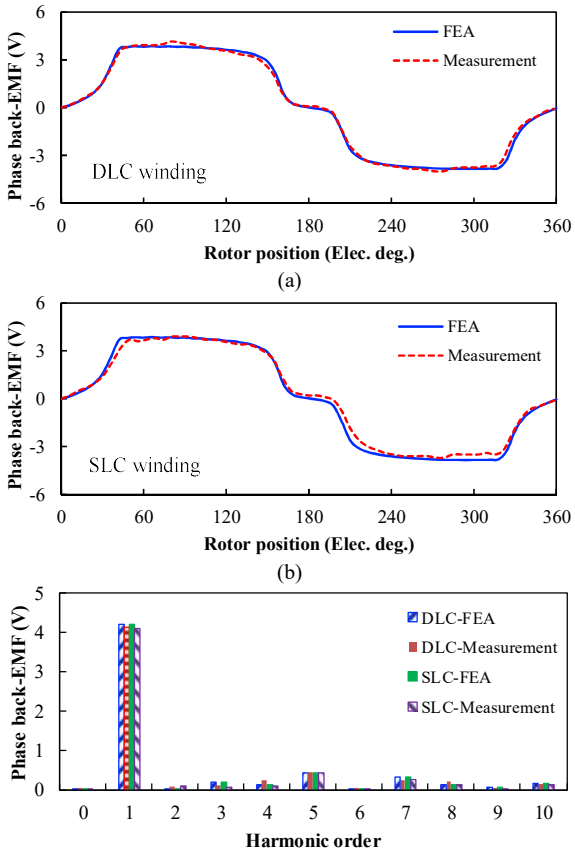

Fig. 16. Measured back-EMFs of 6/4 VFRMs with DLC and SLC winding (DC current is 1A, 400rpm). (a) DLC winding. (b) SLC winding. (c) Spectra.

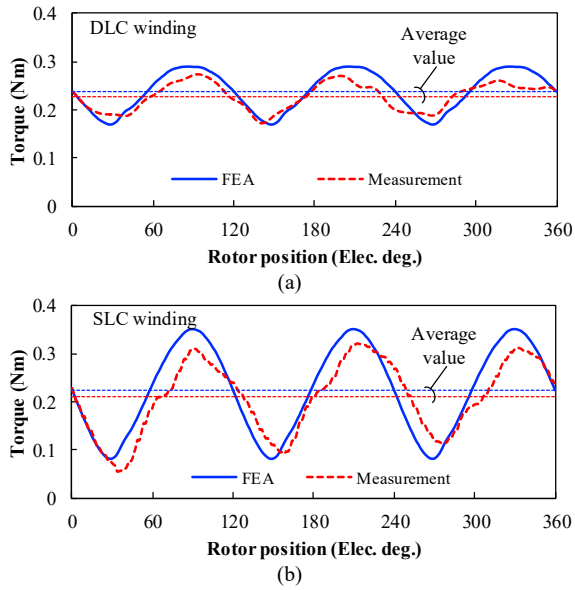

Fig. 17. Measured torque waveforms of 6/4 VFRMs with DLC and SLC winding (DC current is 1.06A, AC current is 1.5A). (a) DLC winding. (b) SLC winding.

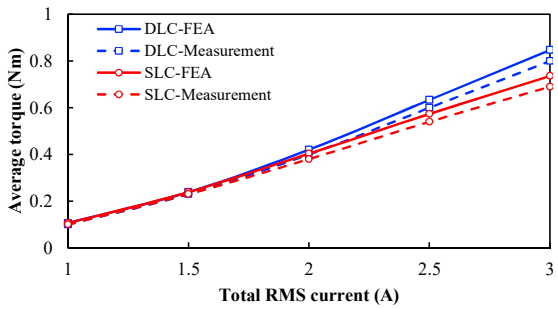

Fig. 18. Variations of average torque against total RMS current of VFRMs with DLC and SLC windings (RMS values of DC and AC currents are equal).

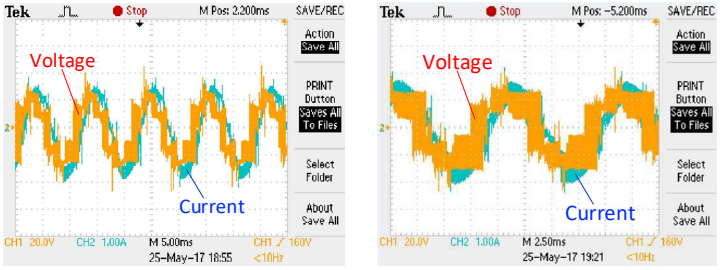

Fig. 19. Voltage and current waveforms measured when rotating speed is 800rpm and total RMS current is 2.1A. (a) VFRM with DLC winding. (b) VFRM with SLC winding.

TABLE IX
COMPARISON OF PREDICTED AND MEASURED EFFICIENCIES OF VFRMS WITH DLC AND SLC WINDINGS

	VFRM with DLC winding		VFRM with SLC winding	
	FEA	Measured	FEA	Measured
400 rpm	47%	40%	43%	38%
800 rpm	64%	56%	59%	51%

VI. CONCLUSION

This paper comparatively analyzes the VFRMs with double- and single-layer windings. It is found that:

(a) All the integers except 3*k* are feasible rotor pole number for both double- and single-layer windings.

(b) The peak value of SLC winding MMF is twice of that of DLC winding, which leads to severe local saturation in VFRMs with SLC winding.

(c) The torque capability of VFRMs with SLC winding is always lower than those with DLC winding. At rated load condition, the VFRMs with SLC winding have 20%~50% lower torque density than those with DLC winding.

(d) The torque ripple of VFRMs with SLC winding is much larger (>2 times) than that of VFRMs with DLC winding due to the additional ripple in reluctance torque.

(e) The VFRMs with SLC winding have larger core loss and lower efficiency than those with DLC winding due to the additional subharmonics in MMF and airgap field.

(f) SLC winding has almost 50% larger phase self-inductance than the DLC winding. Also, it has physical separation between phases. Both aspects lead to better fault tolerance for VFRMs with SLC winding.

Overall, the double-layer winding is superior to single-layer winding and is the preferable choice for VFRMs.

REFERENCES

[1] I. Boldea, L. N. Tutelea, L. Parsa, and D. Dorrell, "Automotive electric propulsion systems with reduced or no permanent magnets: an overview," *IEEE Trans. Ind. Electron.*, vol. 61, no. 10, pp. 5696-5711, Oct. 2014.

[2] T. Fukami, Y. Matsuura, K. Shima, M. Momiyama, and M. Kawamura, "Development of a low-speed multi-pole synchronous machine with a field winding on the stator side," in *Proc. Int. Conf. Elect. Mach.*, Rome, Italy, 2010, pp. 1–6.

[3] X. Liu, Z. Q. Zhu and Z. P. Pan, "Analysis of electromagnetic torque in sinusoidal excited switched reluctance machines having DC bias in excitation," in *Proc. Int. Conf. Elect. Mach.*, Sept. 2012, pp. 2882-2888.

[4] L.R. Huang, J.H. Feng, S.Y. Guo, J.X. Shi, W.Q. Chu, and Z.Q. Zhu, "Analysis of torque production in variable flux reluctance machine," *IEEE Trans. Energy Convers.*, vol. 32, no.4, pp. 1297-1308, Apr. 2017.

[5] X. Liu and Z. Q. Zhu, "Stator/rotor pole combinations and winding configurations of variable flux reluctance machines," *IEEE Trans. Ind. Appl.*, vol. 50, no. 6, pp. 3675–3684, Nov. 2014.

[6] X. Liu, Z. Q. Zhu, M. Hasegawa, A, Pride, and R. Deodhar, "Vibration and noise in novel variable flux reluctance machine with DC-field coil in stator," in *Proc. Int. Conf. Power Electron. Motion Control*, Jun. 2012, pp.1100-1107.

[7] J. T. Shi, X. Liu, D. Wu, and Z. Q. Zhu, "Influence of stator and rotor pole arcs on electromagnetic torque of variable flux reluctance machines," *IEEE Trans. Magn.*, vol. 50, no. 11, pp. 1-4, Nov. 2014.

[8] S. Jia, R. Qu, and J. Li, "Design considerations and parameter optimization of stator wound field synchronous machines based on magnetic the gear effect," in *Proc. IEEE Conf. Energy Convers. Congr. Expo.*, Montreal, QC, Canada, Sep. 2015, pp. 5195–5202.

[9] S. Jia, R. Qu, and J. Li, "Analysis of the power factor of stator DC-excited vernier reluctance machines," *IEEE Trans. Magn.*, vol. 51, no. 11, Nov. 2015, Art. no. 8207704.

[10] X. Liu, Z. Q. Zhu, and D. Wu, "Evaluation of efficiency optimized variable flux reluctance machine for EVs/HEVs by comparing with interior PM machine," *in Proc. 17th ICEMS*, Oct. 2014, pp. 2648–2654.

[11] J. Bao, B. L. I. Gysen, K. Boynov, J. Paulides, and E. A. Lomonova, "Torque ripple reduction for 12-stator/10-rotor-pole variable flux reluctance machines by rotor skewing or rotor teeth non-uniformity," *IEEE Trans. Magn.*, DOI: 10.1109/TMAG.2017.2712609

[12] Z. Q. Zhu, B. Lee, and X. Liu, "Integrated Field and Armature Current Control Strategy for Variable Flux Reluctance Machine Using Open Winding," *IEEE Trans. Ind. Appl.*, vol. 52, pp. 1519-1529, Mar./Apr. 2016.

[13] T. Husain, Y. Sozer, and I. Husain, "DC-assisted bipolar switched reluctance machine," *IEEE Trans. Ind. Appl.*, vol. 53, no. 3, pp. 2098-2109, May/Jun. 2017.

[14] D. Ishak, Z. Q. Zhu, and D. Howe, "Comparison of PM brushless motors, having either all teeth or alternate teeth wound," *IEEE Trans. Energy Convers.*, vol. 21, no. 1, pp. 95–103, Mar. 2006.

[15] P. Reddy, A. El-Refaie, and K. Huh, "Effect of number of layers on performance of fractional-slot concentrated-windings interior permanent magnet machines," *IEEE Trans. Power Electron.*, vol. 30, no. 4, pp. 2205–2218, Apr. 2015.

[16] R. Owen, Z. Q. Zhu, A. Thomas, G. Jewell, and D. Howe, "Alternate poles wound flux-switching permanent-magnet brushless AC machines," *IEEE Trans. Ind. Appl.*, vol. 46, no. 2, pp. 790–797, Mar./Apr. 2010.

[17] W. Hua, H. Hua, N. Dai, G. S. Zhao, and M. Cheng, "Comparative study of switched reluctance machines with half-and full-teeth-wound windings," *IEEE Trans. Ind. Electron.,* vol. 63, no. 3, pp. 1414–1424, Feb. 3, 2016.

[18] X. Y. Ma, G. J. Li, G. W. Jewell, Z. Q. Zhu, and H. L. Zhan, "Performance comparison of doubly salient reluctance machine topologies supplied by sinewave currents," *IEEE Trans. Ind. Electron.*, vol. 63, no. 7, pp. 4086–4096, Jul. 2016.

[19] Z. Zhu, Y. Zhou, J. Chen, and J. Green, "Investigation of nonoverlapping stator wound-field synchronous machines," *IEEE Trans. Energy Convers.*, vol. 30, no. 4, pp. 1420–1427, Dec. 2015.

[20] L.R. Huang, J.H. Feng, S.Y. Guo, J.X. Shi, and Z.Q. Zhu, "Comparative analysis of variable flux reluctance machines with double- and single-layer concentrated armature windings," in *International Conference on Ecological Vehicles and Renewable Energies* (EVER), Apr. 2018, pp. 1-8.

[21] J. A. Walker, D. G. Dorrell, and C. Cossar, "Flux-linkage calculation in permanent-magnet motors using the frozed permeabilities method," *IEEE Trans. Magn.,* vol. 41, no. 10, pp. 3946–3948, Oct. 2005.

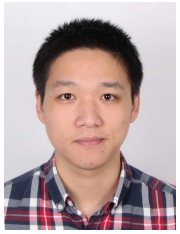

L.R. Huang received the B.Eng. and M.Sc. degrees in electrical engineering from Zhejiang University, Hangzhou, China, in 2012 and 2015, respectively, and the Ph.D. degree in electrical and electronic engineering from The University of Sheffield, Sheffield, U.K., in 2018. Since 2018, he is working as research assistant in Sheffield Siemens Gamesa Renewable Energy Research Centre.

His major research interests include design and application of reluctance machines and permanent magnet machines.

Z.Q. Zhu (M'90–SM'00–F'09) received the B.Eng. and M.Sc. degrees in electrical and electronic engineering from Zhejiang University, Hangzhou, China, in 1982 and 1984, respectively, and the Ph.D. degree in electrical and electronic engineering from The University of Sheffield, Sheffield, U.K., in 1991.

Since 1988, he has been with The University of Sheffield, where he is currently a Professor with the Department of Electronic and Electrical Engineering, Head of the Electrical Machines and Drives Research Group, Royal Academy of Engineering/Siemens Research Chair, Academic Director of Sheffield Siemens Wind Power Research Centre, Director of Sheffield CRRC Electric Drives Technology Research Centre, Director of Midea Electrical Machines and Controls Centre. His current major research interests include the design and control of permanent-magnet brushless machines and drives for applications ranging from automotive through domestic appliances to renewable energy.

Prof. Zhu is a Fellow of Royal Academy of Engineering, UK.

J.H. Feng (S'06) received his B.S. and M.S. degrees in Electrical Machinery Control from Zhejiang University, China in 1986 and 1989, respectively, and Ph. D. degree in Control Theory and Control Engineering from Central South University, China in 2008. Since 1989, he has been with CRRC Zhuzhou Institute Co. Ltd., Zhuzhou, China, where he is presently the Vice President and Chief Technology Officer. He has published a number of journal and conference proceedings papers. His research interests are modeling, control, and communication of

electrical systems, rail networks and high-speed trains. He is also a Guest Professor in Southwest Jiaotong University, Tongji University and Central South University.

S.Y. Guo is a professorial senior engineer. She got graduated from Central South University in December 1981, and serves as the chief technical expert in CRRC Zhuzhou Institute Co., Ltd. in the field of R&D of the electric machine systems for railway locomotive and electrical vehicle.

J.X. Shi received the B. Eng. and M. Sc. degrees in electrical engineering from South China University of Technology, Guangzhou, China in 2010 and 2013, respectively. Since 2013, he has been with CRRC Zhuzhou Institute Co., Ltd.

His major research interests include design and application of permanent magnet machines for electrical vehicle applications.